5850–5860 *Nucleic Acids Research, 2018, Vol. 46, No. 11* *Published online 8 May 2018*
doi: 10.1093/nar/gky323

The structure of the TsaB/TsaD/TsaE complex reveals an unexpected mechanism for the bacterial t^{6}A tRNA-modification

Sophia Missoury[1], Stéphane Plancqueel[1], Ines Li de la Sierra-Gallay[1], Wenhua Zhang[1], Dominique Liger[1], Dominique Durand[1], Raoudha Dammak[1], Bruno Collinet[1,2,*] and Herman van Tilbeurgh[1,*]

[1]Institute for Integrative Biology of the Cell (I2BC), CEA, CNRS UMR 9198, Univ. Paris-Sud, Université Paris-Saclay, 91198 Gif sur Yvette Cedex, France and [2]Institut de Minéralogie, de Physique des Matériaux et de Cosmochimie, UMR7590 CNRS/Sorbonne-Université, UPMC, Paris, France

Received March 12, 2018; Revised April 09, 2018; Editorial Decision April 11, 2018; Accepted April 17, 2018

ABSTRACT

The universal *N*^{6}-threonylcarbamoyladenosine (t^{6}A) modification at position A37 of ANN-decoding tRNAs is essential for translational fidelity. In bacteria the TsaC enzyme first synthesizes an L-threonylcarbamoyladenylate (TC-AMP) intermediate. In cooperation with TsaB and TsaE, TsaD then transfers the L-threonylcarbamoyl-moiety from TC-AMP onto tRNA. We determined the crystal structure of the TsaB–TsaE–TsaD (TsaBDE) complex of *Thermotoga maritima* in presence of a non-hydrolysable AMPCPP. TsaE is positioned at the entrance of the active site pocket of TsaD, contacting both the TsaB and TsaD subunits and prohibiting simultaneous tRNA binding. AMPCPP occupies the ATP binding site of TsaE and is sandwiched between TsaE and TsaD. Unexpectedly, the binding of TsaE partially denatures the active site of TsaD causing loss of its essential metal binding sites. TsaE interferes in a pre- or post-catalytic step and its binding to TsaBD is regulated by ATP hydrolysis. This novel binding mode and activation mechanism of TsaE offers good opportunities for antimicrobial drug development.

INTRODUCTION

Transfer RNAs (tRNAs) are subjected to considerable post-translational processing (1) and today >90 chemical modifications in tRNAs have been characterized (2). The *N*^{6}-threonylcarbamoyladenosine (t^{6}A) modification at position 37 of ANN-decoding tRNAs is one of the few modifications that are found in the three domains of life (3–5). Studies using oocytes demonstrated that A37 and U36 are strictly necessary for t^{6}A formation (6). The t^{6}A base in *Escherichia coli* tRNA^{Lys} stacks with its adjacent A38 and forms a cross-strand stack with the first base of the codon on the mRNA, contributing to the translational fidelity (7). Mutations within the t^{6}A modification pathway compromise anticodon–codon interaction, creating erroneous selection of start codons and aberrant frameshifts. They result in pleiotropic phenotypes and some mutations in human were recently associated with severe neurodegenerative and renal-neurological diseases (8,9). Although the modification is known for >40 years, the t^{6}A biosynthesis enzymes and pathways have only recently been discovered (10–15). t^{6}A biosynthesis is composed of two main steps (schematized in Figure 1): in the first, members of the universal TsaC/TsaC2 (YrdC/Sua5) protein family synthesize an unstable threonylcarbamoyladenylate (TC-AMP) intermediate from *L*-threonine, bicarbonate and adenosine triphosphate (ATP); the second step consists of the transfer of the threonylcarbamoyl (TC) moiety from TC-AMP onto A37 of substrate tRNA. In bacteria, The TC-transfer is carried out by the universal TsaD enzyme (YgjD in *E. coli*) assisted by two other proteins that are present in almost all bacteria: TsaB (YeaZ in *E. coli*) and TsaE (YjeE in *E. coli*). In archaea and eukaryotes, the TC-transfer reaction is carried out by the KEOPS multi-protein complex, composed of Kae1 (the TsaD orthologue), Bud32 (a small protein kinase), Cgi121 and Pcc1, complemented by a fifth protein (16–20) (Gon7 in yeast and C14ORF142 in human). Although TsaD/Kae1 is carrying the TC-transfer activity, the presence of the other subunits are mandatory for the reaction (exception made for Cgi121). In contrast, the yeast mitochondrial TsaD orthologue, Qri7, is capable of, if provided with TC-AMP, modi-

*To whom correspondence should be addressed. Email: herman.van-tilbeurgh@u-psud.fr
Correspondence may also be addressed to Bruno Collinet. Email: Bruno.collinet@i2bc.paris-saclay.fr
Present address: Wenhua Zhang. School of Life Sciences, Lanzhou University, 730000 Lanzhou, China.

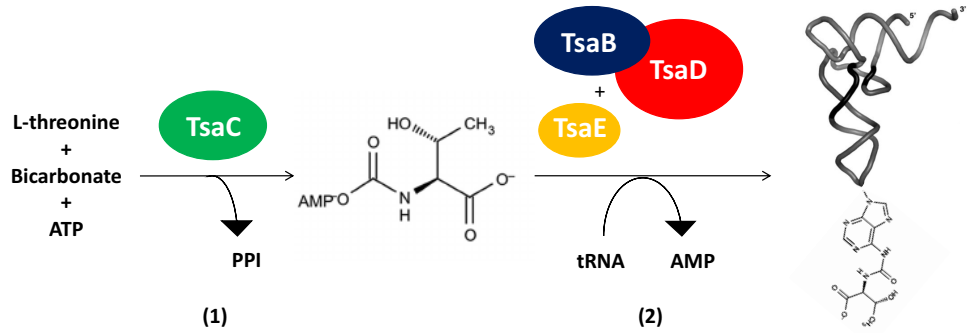

Figure 1. Reaction scheme for t^6A synthesis in bacteria. TsaC uses L-threonine, bicarbonate and ATP for the synthesis of a very unstable TC-AMP intermediate. TsaBD and TsaE then collaborate to transfer the TC-moiety from TC-AMP onto the A37 of tRNA substrates.

fying tRNA *in vitro* without assistance of ancillary proteins (12).

The biochemical function of the ancillary proteins involved in the t^6A pathway is largely unknown, especially the contributions of the TsaE ATPase (bacteria) and the Bud32 kinase (archaea/eukaryotes) to the t^6A synthesis reaction remains enigmatic. TsaB is a paralogue of TsaD that has lost its catalytic function and TsaE belongs to a large class of nucleotide hydrolases. TsaD physically interacts with TsaB and TsaE and their genes are often clustering (15,21–23). The crystal structures of the heterodimeric TsaBD (22,24) showed that TsaB and TsaD associate via hydrophobic packing of 2 two pairs of N-terminal helices into a helical bundle, mimicking the structure of homodimeric TsaB (25,26) and Qri7 (12). Although Pcc1 is unrelated to TsaB, a similar helical bundle is also found at the Kae1–Pcc1 heterodimer interface (27). Except for some intracellular or symbiotic organisms (e.g. *Mycoplasma*), TsaE is present in all bacteria (3). TsaE has an intrinsically weak ATPase activity that is strongly activated by its binding to the TsaBD complex regardless of the presence of other substrates for the biosynthesis of tRNA t^6A (22–24). The need of ATP-hydrolysis for t^6A biosynthesis in bacteria is presently unclear. The structure of TsaE in complex with ADP revealed the presence of a Walker A motif and two switch regions that are characteristic of P-loop GTP hydrolases (28,29) In presence of non-hydrolysable ATP analogues, *Ec*TsaB, *Ec*TsaD and *Ec*TsaE form a *Ec*TsaBDE complex with 1:1:1 stoichiometry (22). From small angle X-ray scattering (SAXS) measurements and biochemical data, it was proposed that *Ec*TsaE binds at the *Ec*TsaBD interface (22). In a very recent manuscript, Luthra *et al.* reported the characterization of the TsaBDE threonylcarbamoyl transfer complex of *T. maritima* (*Tm*TsaBDE) (23). Their SAXS analysis revealed that *Tm*TsaBDE forms a symmetric hexameric quaternary assembly in solution with 2:2:2 stoichiometry ($TmTsaB_2D_2E_2$). This hexamer turned out to be a dimer of *Tm*TsaBDE heterotrimers, with *Tm*TsaB acting as a dimerization module, reminiscent of Pcc1 in eukaryotic and archaeal KEOPS (30,31). *Tm*TasB and *Tm*TsaD were further shown to form a $TmTsaB_2D_2$ complex that was capable to bind one tRNA molecule, and accommodate a single TsaE subunit. Quantitative activity measurements demonstrated that $TmTsaB_2D_2$ alone can catalyse only a single round of t^6A synthesis (23). An ensemble of kinetic and binding experiments led to the hypothesis that *Tm*TsaE-catalyzed ATP hydrolysis occurs after the release of the t^6A-modifed tRNA (23).

The essential character of TsaE for bacterial survival, the presence of its encoding gene in all pathogenic bacterial genomes and the absence of human orthologues, makes TsaE an attractive antibacterial drug target (29,32). However, its role in the t^6A process remains poorly understood, mainly because there is no high resolution structural information on its interactions with TsaBD. In this manuscript we present the X-ray structure of the *Tm*TsaBDE complex bound to AMPCPP at 3.1 Å resolution. *Tm*TsaE is bound at the interface of *Tm*TsaBD, making asymmetric contacts with *Tm*TsaB and *Tm*TsaD. The AMPCPP nucleotide was found sandwiched between *Tm*TsaE and *Tm*TsaD with its γ-phosphate group being coordinated by side chains from both subunits. Crystallographic symmetry generates the hexameric $TmTsaB_2D_2E_2$ complex that was proposed to be present in solution (23). Surprisingly, *Tm*TsaE partially denatures the active site of *Tm*TsaD and prevents simultaneous substrate tRNA binding, suggesting that *Tm*TsaE is required for a reaction step before or after the TC-transfer from TC-AMP to tRNA.

MATERIALS AND METHODS

Expression and purification of the TmTsaBDE subunits

We prepared the *Tm*TsaBD binary complex and the *Tm*TsaE protein individually. A bicistronic expression vector (named BC14) aimed to co-express *Tm*TsaD and *Tm*TsaB-His was designed as described (33). All synthetic gene constructs were optimized according to *E. coli* codon usage using the EuGene software (34) (Supplementary Table S2) and obtained from Genscript (Piscataway, USA). The DNA sequences coding for *Tm*TsaD and *Tm*TsaB containing a 6His-tag at the C-terminus have been cloned into a pET21a backbone using the NdeI and XhoI restriction sites. The second vector (named BC15) aimed to express *Tm*TsaE-Nt-his was cloned into a pET24d backbone between NcoI and XhoI restriction sites. This plasmid, was used to express *Tm*TsaE with a N-terminal 6His-tag followed by a TEV proteolytic recognition site to remove the 6his-tag if necessary. *Tm*TsaD and *Tm*TsaB-His have been

co-expressed in *E. coli* Rosetta pLysS strain transformed with the BC14 plasmid and grown at 37°C in 2xYT liquid medium supplemented with ampicillin and chloramphenicol until mid-log phase. Expression was induced by adding 0.5 mM isopropyl β-D-1-thiogalactopyranoside and the cells were incubated for three more hours at 37°C and then harvested by centrifugation, re-suspended in lysis buffer (20 mM Tris–HCl pH 7.5, 200 mM NaCl), and stored at −20°C until purification. The same protocol was followed for the expression of *Tm*TsaE, using plasmid BC15 and tetracycline antibiotic instead of ampicillin.

For purification, cells were thawed at 25°C and lysed by sonication (Branson Sonifier 250) on ice-cold water and centrifuged at 20 000 g for 30 min. Supernatant was applied onto NiIDA resin (Qiagen) previously equilibrated with Tris–HCl buffer (25 mM Tris–HCl pH 7.5, 200 mM NaCl, 5 mM 2-mercaptoethanol). Resin was washed with 20 ml of the same buffer and the proteins were eluted using three fractions of 4 ml of the previous buffer supplemented with 100, 200 and 400 mM imidazole. Fractions containing the proteins of interest were pooled and concentrated by ultra-filtration and loaded on superdex 75 (GE-Healthcare) equilibrated in HEPES buffer (20 mM HEPES pH 7.5, 200 mM NaCl, 5 mM 2-mercaptoethanol).

Finally, fractions containing the proteins of interest were pooled and concentrated to 50 mg.ml^{-1} or 60 mg.ml^{-1} for *Tm*TsaE and *Tm*TsaBD respectively. Purity was checked by SDS-PAGE.

Crystal structure determination

Purified *Tm*TsaBD *and Tm*TsaE were mixed at a 1:1:1 ratio of the three subunits up to a final concentration of 12 mg.ml^{-1} (0.148 mM) in HEPES buffer 20 mM pH 7.5, 200 mM NaCl, 5 mM 2-mercaptoethanol supplemented with 3 mM AMPCPP and 6 mM $MgCl_2$. Crystals of *Tm*TsaBDE were obtained at 293 K using the sitting-drop vapour diffusion method by mixing 100 nL of a protein solution with 100 nl of 13% PEG 8000, 0.1 M Imidazole pH 7.35. Crystals were cryoprotected with reservoir solution supplemented with 30% glycerol and 3mM AMPCPP, flash-frozen and stored in liquid nitrogen for data collection. X-ray diffraction data collection was carried out on beamline Proxima2 at the SOLEIL Synchrotron (Saint-Aubin, France) at 100K. Data were processed, integrated and scaled with the XDS program package (35). *Tm*TsaBDE crystals belonged to space group $P2_12_12_1$ with unit cell parameters of $a = 84.31$ Å, $b = 113.94$ Å, $c = 177.62$ Å. The structure of *Tm*TsaBDE was solved by molecular replacement using the PHASER module (36) implemented in the CCP4 software package (37). Search models for *Tm*TsaB and *Tm*TsaD were obtained by the MODELLER program (38) using the crystal structure of the *Ec*TsaBD heterodimer (PDB ID: 4YDU) and *Tm*TsaE was modelled from the *Hi*TsaE structure (PDB ID: 1FL9). The initial structure was refined using the PHENIX program (39) and completed by interactive and manual model building using COOT (40). Two copies of the *Tm*TsaBDE trimer were present in the asymmetric unit. AMP-CPP molecules and $MgCl_2$ ions could be modeled into the residual Fo-Fc electron density contoured at 3.0σ. Data collection and refinement statistics are gathered in Table 1.

tRNA docking

The *Ec*TsaDB-tRNA complex model was generated by rigidly docking a tRNA molecule onto the *Ec*TsaBD complex using the HADDOCK Server (version 2.2) (41). The tRNA structure was extracted from the crystal structure of threonyl-tRNA synthetase-tRNA complex (PDB : 1QF6) (42) in which the *E. coli* $tRNA^{Thr}$ UGC contains a m^6t^6A at position 37 in the anticodon loop. For docking, the m^6t^6-moeity and other modifications were removed from the E. coli $tRNA^{Thr}$ UGC. The docking protocols and parameters follow the default settings for protein-RNA complexes in HADDOCK. As for the direct contact sites, critically, His111 and His115 in *Ec*TsaD were specified as active site residues in the receptor molecule whereas A37 was specified as substrate in tRNA. By default, the active sites-surrounding residues were specified as passive. Resulting models were ranked based on scoring performance and clustered. The first model from the top-ranked cluster was chosen to represent the structures.

Sequence alignment and structure comparison

The sequence conservation was analysed using the program CONSURF (43) with *Tm*TsaBDE as the query. The frequency of the occurrence of amino acids on the consensus sequence was produced by WebLogo (44). Structural comparison was performed with the PDBeFold web server (45). All graphic structure representations were produced with PYMOL (46). The electrostatic potential representation were rendered and produced by PDB2PQR (47) and APBS in the Chimera visualization system (48).

RESULTS AND DISCUSSION

Overall structure of the TmTsaBDE complex

We obtained diffracting crystals of *Tm*TsaBDE only in the presence of AMPCPP and the structure was solved at 3.14 Å resolution. The asymmetric unit of the crystals contains two copies of a *Tm*TsaBDE trimer, whose structures are very similar (all RMSD values for superimposed structures are gathered in Supplementary Table S1).

The overall structures of *Tm*TsaB, *Tm*TsaD and *Tm*TsaE in the complex are the same as those of the individual proteins (*Tm*TsaB) or orthologues (*H. influenza (Hi)*- and *B. subtilis(Bs)*TsaE and *St(S. typhimurium)*, *Ec(E. coli)*TsaD and Kae1) (Supplementary Table S1) (28,29) (49). Sequence alignments with superposed secondary structure assignments of a few TsaB, TsaD and TsaE orthologues are represented in Supplementary Figure S1. As illustrated in Figure 2a, *Tm*TsaB and *Tm*TsaD embrace *Tm*TsaE to form a compact ternary complex, in agreement with SAXS measurements on *Ec*- and *Tm*TsaBDE in solution (22,23). *Tm*TsaE is held in a grip between the helical insertion of the C-terminal domain of *Tm*TsaD on one side and *Tm*TsaB on the other. *Tm*TsaE establishes two main contacts with *Tm*TsaBD. The first involves the α3-helix (residues 90–100)

Table 1. Crystallographic data-collection and refinement statistics of TmTsaBDE

X-ray source	PROXIMA 2
Wavelength (Å)	0.9801
Temperature (K)	100
Unit-cell parameters (Å, °)	$a = 84.31$, $b = 113.94$, $c = 177.62$, $\alpha = \beta = \gamma = 90.0$
Space group	$P2_12_12_1$
Resolution limits[a] (Å)	48.44 – 3.14 (3.33–3.14)
Number of observations[a]	138146 (21963)
Number of unique reflections	30297 (4627)
R-meas[a] (%)	19.1 (149.7)
Completeness[a] (%)	99.1 (95.2)
I/σ (I)[a]	7.1 (1.03)
CC (1/2)[a] (%)	99.2 (43.9)
Number of non-hydrogen atoms (proteins/ligands)	10418/77
R/R_{free} (%)	22.58/29.37
R.M.S.D. Bonds (Å)/angles (°)	0.010/1.258
Average B-factor (proteins/ligands)	80.67/80.91

[a]Values in parentheses refer to the highest resolution shell.

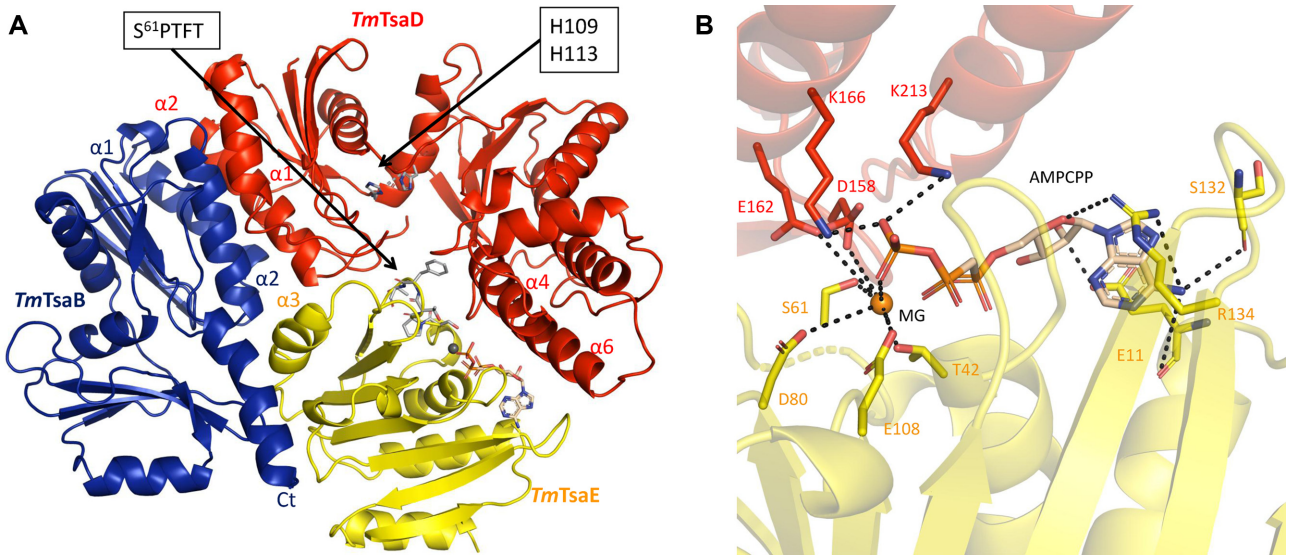

Figure 2. Structure of *Tm*TsaBDE. (**A**) Ribbon diagram of *Tm*TsaBDE (*Tm*TsaB: blue, *Tm*TsaD: red, *Tm*TsaE: yellow). The main structural elements involved in protein interfaces are indicated following the colour codes of the individual proteins (*Tm*TsaBD : α1 and α2 from *Tm*TsaB and *Tm*TsaD; *Tm*TsaDE: α4 and α6 from *Tm*TsaD and loops from *Tm*TsaE). The two histidines (His109 and His113) in the active site of *Tm*TsaD responsible for metal binding and the S^{61}PTFT motif of *Tm*TsaE are indicated by an arrow. AMPCPP at the interface between *Tm*TsaD and *Tm*TsaE is represented by sticks. The Mg-ion boud to AMPCPP is represented as a grey sphere. (**B**) AMPCPP binding site. *Tm*TsaE in yellow and *Tm*TsaD in red, AMPCPP is in sticks, Mg-ion as orange sphere. Side chains in H-bond interaction with the AMPCPP γP group are represented as sticks.

of *Tm*TsaE that binds to the N-terminal end of the four-helical bundle of the TsaBD interface. The α3-helix is partially disordered in *Bs*TsaE and forms two short perpendicularly oriented helices in *Hi*TsaE (illustrated in Supplementary Figure S2). This helix and the connection between β5 and β6 (residues 115–120) contact both N- and C-terminal domains of *Tm*TsaB. The second main contact between *Tm*TsaE and *Tm*TsaBD is provided by the loops emanating from the C-terminal end of the parallel section of the *Tm*TsaE β-sheet and the helical insertion in the C-terminal domain of *Tm*TsaD, englobing the AMPCPP ligand (Figure 2A and Supplementary Figure S8). The totally conserved *Tm*TsaE peptide S^{61}PT(F/Y)T, dips into the active site of *Tm*TsaD, containing two essential histidines (His109 and His113, highlighted in Figure 2A). This peptide contacts α4 and the hairpin connection between β6 and β7 of *Tm*TsaD, forming H-bonds between well conserved residues (Supplementary Figure S1). The loop between β6 and β7 sandwiches the γP-group of ATP in its complex with *St*TsaBD (24). Since the S^{61}PT(F/Y)T motif is also involved in a H-bond network with the γP-group of AMPCPP, this loop could be a communicator between the compound bound in the active site of TsaD and the ATP binding site on TsaE (see discussion in mechanism section).

The *Tm*TsaB C-terminus is elongated and disordered beyond residue 194 in one copy of the asymmetric unit, while in the other it forms a helix comprised between residues 190 and 203. We showed that the C-terminal peptide of *Ec*TsaB is not required for formation of the binary *Ec*TsaBD complex (22), but it might contribute to the stability of *Ec*TsaBDE. The regions involved in these contacts

are very poorly conserved, suggesting that they are not a major determinant for TsaE binding.

Although TsaB and TsaD have the capacity *in vitro* of forming homodimers whose quaternary structures are very similar to the TsaBD heterodimer, individually they do not interact with TsaE (22,23). Although there is no structure of the TsaD homodimer available, it likely resembles its mitochondrial orthologue Qri7, whose homodimer assembly is very similar to that of TsaB (12). *Tm*TsaE is engaged in a totally asymmetric interaction with *Tm*TsaB and *Tm*TsaD, explaining why TsaE binds neither TsaB nor TsaD homodimers (22).

AMPCPP binds at the interface between TmTsaD and TmTsaE

After initial refinement of the molecular replacement solution, a consistent cloud of residual electron density was identified at the expected nucleotide-binding site of *Tm*TsaE. As shown in Supplementary Figure S4, this density could be fitted by AMPCPP, whose presence was mandatory for obtaining diffracting crystals. Residual electron density was also present for a Mg^{2+} ion, coordinated by the β- and γ-phosphate groups of AMPCPP, Thr42$^{O\gamma}$ and Glu108^{COO-}. AMPCPP is located at the C-terminal edge of the parallel strands of the central β-sheet. Most remarkably, AMPCPP is sandwiched between *Tm*TsaE and the helical insertion of the C-terminal domain of *Tm*TsaD that partially seals off its polyphosphate. The AMPCPP nucleotide adopts an unusual syn-conformation and overlaps with ADP in complex with *Hi*TsaE and *Bs*TsaE (28,29) (Supplementary Figure S2). *Tm*TsaE binds AMPCPP in a manner globally observed in other P-loop proteins (Figure 2B). The N^6 atom of adenine hydrogen bonds to main chain atoms of Ser132 and Glu11 and the base-ring is stacked between the side chains of Glu11 and Arg134, which also hydrogen bonds with the ribose O^4. The ribose O^2 hydrogen bonds with the Glu11 carboxylate and the ribose O^3 establishes a H-bond with the main chain carbonyl of *Tm*TsaD Phe116. The phosphate moieties of AMPCPP make classic hydrogen contacts with the *Tm*TsaE P-loop (G^{38}AGKTT) at the N-terminus of α2. *Ec*TsaE does not bind to *Ec*TsaBD in presence of ADP (22) and the affinity of *Tm*TsaE for *Tm*TsaBD drops fourfold in absence of ATP (23). It was also shown that the basal low ATPase activity of *Ec*TsaE is boosted by the presence of *Ec*TsaBD (22). These observations can be explained by the fact that the position of the AMPCPP γP-group is stabilized by salt bridge formation with the conserved Lys166 and Lys213 from *Tm*TsaD (Figure 2B). Lys166$^{N\zeta}$ also hydrogen-bonds with Thr63$^{O\gamma H}$ that is part of the totally conserved SPT motif in contact with the *Tm*TsaD active site. The carboxylate group of the totally conserved *Tm*TsaE Asp80 is at ∼5 Å from the γP of AMPCPP, ideally positioned to act as a general base for ATP hydrolysis. It was noticed that this Asp is part of a conserved HxD(L/V)YR motif that was reminiscent of Hanks type kinases (29,51). Mutation of the homologous Asp80 in *Bs*TsaE annihilated its (auto)phosphorylation activity.

Different effects of ATP nucleotides on the binding of TsaE to TsaBD have been observed for different organisms. *Tm*TsaE is able to bind *Tm*TsaBD in absence of added nucleotides with an affinity constant of 1.3 μM, which decreases about 4-fold in presence of ATP, while ADP has no effect (23). Two active-site mutants defective in ATP binding, *Tm*TsaE^{T42A} and *Tm*TsaE^{E108A}, preserved their binding to *Tm*TsaBD (23). *Ec*TsaE does not bind to *Ec*TsaBD in absence of ATP but binds with 1:1:1 stoichiometry and a 0.6 μM K_d in presence of Mg^{2+} and AMPPNP (22). *Ec*TsaE^{T43A} and *Ec*TsaE^{E108A} mutants (also defective in binding to ATP or ADP) did not interact with *Ec*TsaBD (22). The strength and ATP dependence of the binding of TsaE to TsaDB probably is species dependent and variations might exist between for instance hyperthermophilic and mesophilic bacteria.

Comparison of TsaE with small GTPases suggested that Tyr82 and Trp109 are part of putative switch regions (Supplementary Figure S2) (22,50). Trp109$^{N\varepsilon1}$ (switch I) hydrogen-bonds with the γP of AMPCPP and Tyr82 (switch II) stacks against TsaD Lys166. *Ec*TsaE^{Y82A} and *Ec*TsaE^{W109A} had ∼7-fold diminished affinity for ATPγS but *Ec*TsaE^{W109A} kept WT binding capacity to *Ec*TsaBD in presence of AMPPNP. Although the *Ec*TsaE^{W109A} mutant had diminished ATPase activity it was active in t^6A biosynthesis. It should be noticed that the conformation of switch regions in small GTPases is usually strongly influenced by the nature of the bound nucleotide (GTP versus GDP) (50), but this is not the case for *Tm*TsaE.

To conclude, AMPCPP binding in *Tm*TsaBDE is conferred by residues both from *Tm*TsaD and *Tm*TsaE. Residues from *Tm*TsaD complete the coordination of the γP group of ATP and hence are likely responsible for the activation of the hydrolytic activity of *Tm*TsaE upon binding to *Tm*TsaBD. Our structure clearly explains in general why ATP is needed for (or increases) the binding of TsaE to TsaBD and why this complex boosts the ATPase activity of TsaE.

TmTsaE binding induces an inactive conformation of TmTsaD

Global superposition of *Tm*- and *Ec*TsaD indicates that the relative positions of the N- and C-terminal domains changes considerably upon formation of the *Tm*TsaBDE complex (Figure 3A). The α3 and α9 helices of *Tm*TsaD at the bottom of the active site shift their positions by ∼4 Å forming the hinge of a rotation that separates the C- and N-terminal domains and opens up the active site cleft. At its periphery the N-terminal domain of *Tm*TsaD moves by ∼11 Å. These observations corroborate reported SAXS data obtained from *Tm*$TsaB_2D_2$ in solution, which were best fitted by an equilibrium population between an open and closed form of *Tm*TsaD (23). The distance between the two *Tm*TsaD units in the 'open form' of *Tm*$TsaB_2D_2$ was estimated to be 85 Å, a value that agrees with the present crystal structure of *Tm*$TsaB_2D_2E_2$. The closed form of *Tm*$TsaB_2D_2E_2$ likely corresponds with the structure of TsaD as observed in the *St*- and *Ec*TsaBD binary complexes.

Apart from pushing the two domains of *Tm*TsaD apart, *Tm*TsaE binding partially 'melts' its active site pocket. Electron density was missing for residues 31–47 of *Tm*TsaD for both copies in the asymmetric unit, suggesting they became

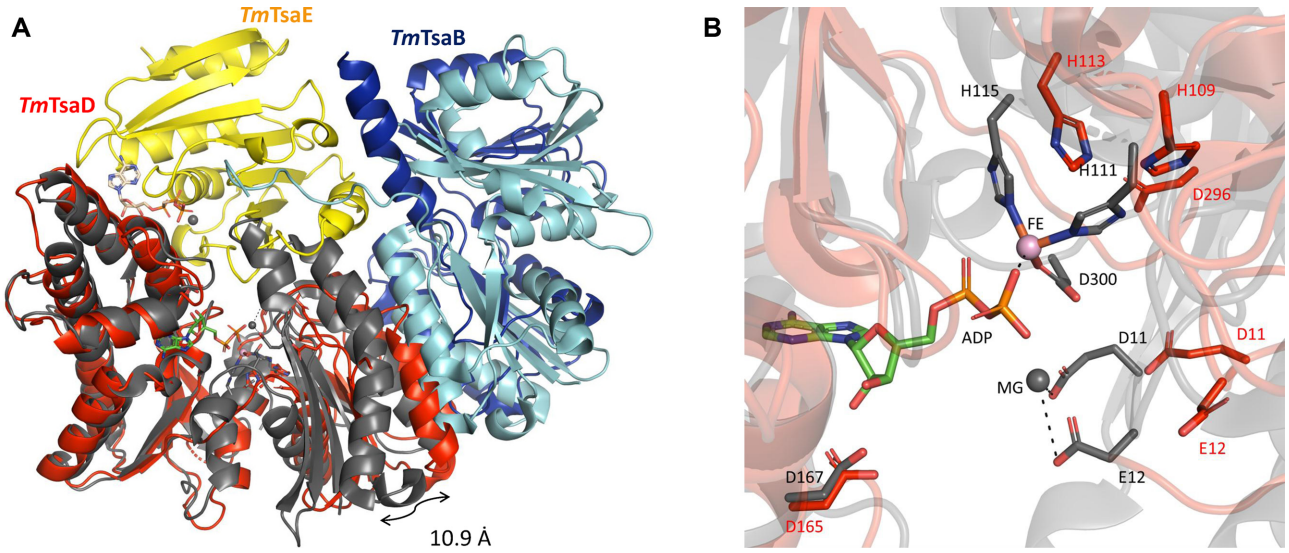

Figure 3. Structure comparison between *Ec*TsaBD and *Tm*TsaBDE. (**A**) Superimposition of *Ec*TsaBD (PDB ID 4YDU; *Ec*TsaB in cyan and *Ec*TsaD in gray) and *Tm*TsaBDE (same colour code as for Figure 2A). The C-terminal domains of TsaD were superimposed. The ADP (bound to *Ec*TsaBD) and the AMPPNP bound to *Tm*TsaE are shown as sticks. As indicated the N-terminal domain position of TsaD shifts by ∼11 Å between *Ec*TsaBD and *Tm*TsaBDE. (**B**) Zoom into the TsaD active site. Superposition of *Ec*TsaBD (gray shadow) and *Tm*TsaBDE (red shadow). Fe- and Mg-binding side chains are shown using the same color code. Fe- and Mg-ions are in pink and grey spheres respectively and ADP is in sticks.

disordered. This peptide region has a well-defined conformation in binary TsaBD complexes: residues 31–39 form a helix (α1) that is collinear with strand β3 and residues 41–47 form the two first helical turns of α2. The superimposition of *Ec*TsaBD and *Tm*TsaBDE onto the TsaD N-terminal domains (Supplementary Figure S5), shows that the structure of this peptide as present in *Ec*TsaBD would create an important steric clash with *Tm*TsaE. A second region of *Tm*TsaD that becomes disordered in *Tm*TsaBDE, is contained between residues 292 and 294. The corresponding peptide in *Ec*TsaBD provides a carboxylate ligand (^{Ec}Asp300) to the Fe-ion. The induction of partial disorder and conformational changes into the *Tm*TsaD active site by the presence of *Tm*TsaE significantly affects the positions of many of the crucial residues involved in AMP and metal binding. Figure 3b illustrates ADP bound in the active site of *Ec*TsaBD (22,24) superposed onto the active site of *Tm*TsaD. The α- and β-phosphates are ligands of a metal ion (Fe in *Ec*TsaBD), which is further coordinated by His111 (^{Tm}His109), His115 (^{Tm}His113) and Asp300 (^{Tm}Asp296). A Mg-ion is positioned at 4 Å away from the α- and β-phosphates of ADP and is coordinated by the Asp11 (^{Tm}Asp11) and Glu12 (^{Tm}Glu12) carboxylates. The opening of the active site pocket and the induced disorder render the metal binding sites of *Tm*TsaD ineffective (Figure 3B): (i) His109 and His113 shifted over >3 Å and are no longer in a configuration capable of binding a metal ion; (ii) the peptide containing the third metal-coordinating residue Asp296 became disordered; (iii) the two Mg-coordinating residues (Asp11 and Glu12) also moved by ∼3 Å away from the polyphosphate moiety position of the nucleotide. Mutations of the homologous histidines in Kae1, renders yeast strains hardly viable and abolishes the t^6A-synthesizing activity (27,31). The *Ec*TsaD^{E12A} mutant is totally inactive, although it is still capable of binding *Ec*TsaE and *Ec*TsaB (22), suggesting that the integrity of the Mg-binding site of TsaD is essential for activity but not for TsaE binding. We conclude that the binding of *Tm*TsaE opens and partially melts the active site of *Tm*TsaD, resulting in an inactive conformation of *Tm*TsaD.

TmTsaE blocks the active site entrance for a tRNA substrate

The biochemical characterization of tRNA binding to TmTsaBDE was recently reported (23). Both *Tm*TsaB$_2$D$_2$ and *Tm*TsaB$_2$D$_2$E are able to bind tRNA with μM affinity, but no tRNA binding was observed for *Tm*TsaB$_2$D$_2$E$_2$. These data corroborated our observations that tRNA did not bind to *Ec*TsaBDE (22). Our structural data explain why TsaE and tRNA are competing for binding to TsaBD: the position of TsaE prevents the access of the anti-codon loop of the bulky tRNA substrate to the TsaD carbamoylation site (centered on the Fe/Mg cluster). The surface projection of the electrostatic potential (Figure 4A) shows that *Tm*TsaBD contains an extensive positively charged groove surrounding the active site pocket, obviously a good candidate for tRNA binding. We modeled a complex of a rigid tRNA substrate with *Ec*TsaBD using the HADDOCK software (41). The tRNA in the HADDOCK model extensively interacts with the positive surface patch present on TsaBD (Figure 4B) and most importantly sterically overlaps with *Tm*TsaE in the *Tm*TsaBDE complex. Electrostatic surface calculation of *Tm*TsaE reveals a negatively charged surface patch centered on the α3 helix that is positioned onto a positively charged patch at the *Tm*TsaBD interface. Although the residues at the interface are not completely conserved, the electronegative character of this region is maintained in the *Ec*-, *Bs*- and *Tm*TsaE homologues (Supplementary Figure S6). TsaE can be considered as an electrostatic competitor of the tRNA substrate.

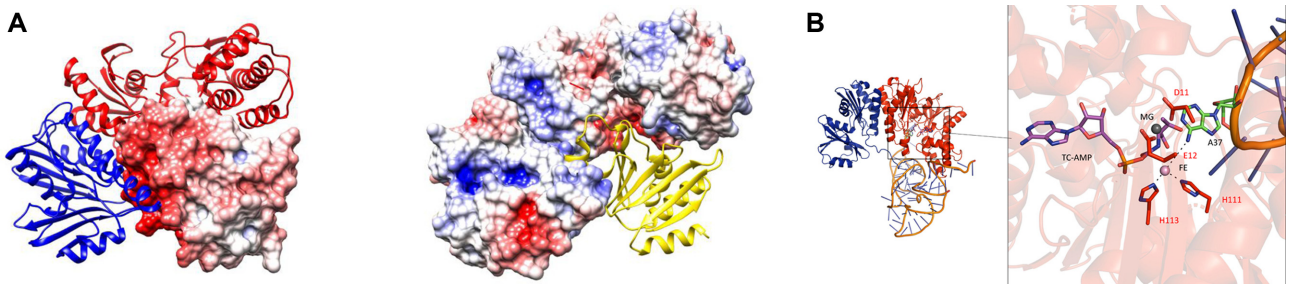

Figure 4. *Tm*TsaE and tRNA binding sites overlap. (**A**) Left panel: the electrostatic potential surface of *Tm*TsaE and ribbon presentation of *Tm*TsaBD; right panel: the electrostatic potential surface of *Tm*TsaBD and ribbon presentation of *Tm*TsaE (negatively and positively charged surfaces are in red and blue respectively). Ribbon presentation uses same colour code as Figure 2A. (**B**) Left panel: the HADDOCK model of *Ec*TsaBD (in ribbon) bound to tRNA; right panel: view of the active site of the modelled *Ec*TsaBD-tRNA-TC-AMP complex. TC-AMP is in sticks. tRNA-A37 is in green sticks and some of the metal ligands are in red sticks. Fe-ion in pink and Mg-ion in gray sphere.

The competition between tRNA and TsaE also explains why the strong ATPase activity upon binding of TsaE to TsaBD is observed independently of tRNA (22,23). In agreement with conclusions from biochemical data (22,23), the *Tm*TsaBDE structure definitely confirms that TsaE must operate in a reaction step that is unrelated to the proper carbamoyl-transfer from TC-AMP onto tRNA A37.

Quaternary structure of *Tm*TsaBDE

The structure of the *Tm*TsaB dimer was previously determined by a structural genomics consortium (25). The crystal packing in that study suggested two possible dimerization modes for *Tm*TsaB. In the first, the β3 strands of the two N-terminal domains align to form an antiparallel extended β-sheet. In the second dimer type, the α1 and α2 helices of the N-terminal domains of each subunit are packed into a four-helical bundle, closely mimicking the helical arrangement observed at the TsaBD interface. Although the latter dimerization has a smaller contact area mode, it was found exclusively in all other TsaB homologue structures (26,52). SAXS analysis of *Tm*TsaBDE demonstrated it forms a heterohexamer in solution consisting of two copies of each subunit ($TsaB_2D_2E_2$) (23). The two copies of the *Tm*TsaBDE trimer in the asymmetric unit do not associate into a hexamer. However, *Tm*TsaB forms a crystal symmetry generated dimer that involves the β3 strands of the two N-terminal domains. Using *Tm*TsaB as the dimerizing subunit, we generated a $TsaB_2D_2E_2$ heterohexamer (Figure 5A) that is very close to the one proposed from SAXS data (23). We confirm that the quaternary structure of the *Tm*TsaBDE complex is different from trimeric *Ec*- and *St*TsaBDE (22–24). Structure imposition reveals that *Ec*- and *St*TsaB have a 19 amino acid insertion in the C-terminal domain compared to *Tm*TsaB, that forms an extra strand and a long helical connection. This insertion is positioned close to the *Tm*TsaB interface region observed in the structures of *Tm*TsaB and *Tm*TsaBDE. Superimposition of the *Ec*- and *St*TsaB monomer structures onto the *Tm*TsaB dimer creates a considerable steric clash between the inserted regions of the two subunits (not shown). Therefore, *Ec*- and *St*TsaB would not be able to adopt the *Tm*TsaB type dimer structure, explaining why *Ec*- and *St*TsaBDE are trimers and not hexamers in solution. This is probably the case for the majority of species, since most TsaB sequences have this C-terminal insertion and we expect that the trimeric TsaBDE complex is the standard configuration.

As discussed above, bacterial TsaBDE adopts different quaternary assemblies according to species. This type of heterogeneity was also observed in the archaeal and eukaryotic systems. Archaeal KEOPS is a dimer of heterotetramers (Pcc1-Kae1-Bud32-Cgi121) (30) while in eukaryotes, a fifth KEOPS subunit (Gon7 in yeast) prevents Pcc1 dimerization and the functional unit is a heteropentamer. In humans, C14ORF142 plays a similar role as Gon7 in yeast and prevents the dimerization of the LAGE3 (the Pcc1 orthologue) subunit (19). In absence of C14ORF142, LAGE3-OSGEP-TPRK-TPRB forms a dimer of heterotetramers.

Activation mechanism of the t^6A activity by TsaE

Kinetic experiments suggested that, in absence of *Tm*TsaE, $TmTsaB_2D_2$ is able to catalyse a single turnover. However, the presence of *Tm*TsaE is required to attain multiple cycles of t^6A activity (23). *Tm*TsaE mutants that have lost their ATPase or *Tm*TsaBD binding activities are incapable of sustaining multiple-round catalysis of the *Tm*TsaD enzyme. On the other hand, the present structure of *Tm*TsaBDE, supported by recent biochemical data (23), proves that *Tm*TsaE and tRNA-substrate cannot simultaneously bind to *Tm*TsaBD. *Tm*TsaE must therefore carry out an essential step on the enzymatic pathway occurring before or after the transfer of the threonylcarbamoyl-moiety from TC-AMP onto A37. Luthra *et al.* suggested that after synthesis of t^6A-tRNA, *Tm*TsaD might be left in an inactive state and *Tm*TsaE-mediated ATP hydrolysis might 'reset' *Tm*TsaD for the next reaction cycle (23). Obviously, to provide access for the tRNA substrate to the active site of *Tm*TsaD, *Tm*TsaE must bind and dissociate from *Tm*TsaBD during the reaction cycle, a process that is likely regulated by its ATPase activity. The affinity of *Tm*TsaE for *Tm*TsaBD is in the micromolar range, and diminishes in absence of ATP (23). For *Ec*TsaE we did not observe binding to *Ec*TsaBD without ATP (22). Apart from playing a regulatory role for tRNA binding, *Tm*TsaE also affects the active site conformation of *Tm*TsaD. *Tm*TsaE perturbs the integrity of the *Tm*TsaD metal-binding sites which are essential for activity and hence induces an inactive state of the *Tm*TsaD enzyme. It is not obvious why *Tm*TsaD should go through a 'denat-

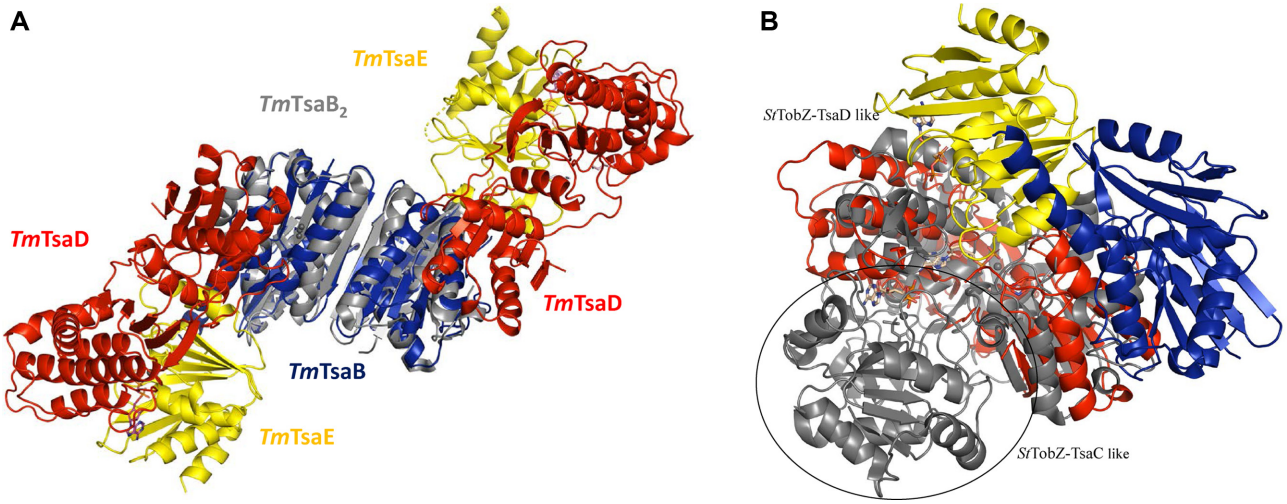

Figure 5. Quaternary structure of *Tm*TsaBDE. (**A**) Ribbon representation of the *Tm*TsaB$_2$D$_2$E$_2$ hexamer, a dimer of *Tm*TsaBDE trimers, that was extracted from the crystal packing. This assembly agrees with the hexamer which was proposed in solution, based on SAXS experiments (23) (*Tm*TsaB: blue, *Tm*TsaD: red, *Tm*TsaE: yellow). *Tm*TsaB forms the central dimerization unit, corresponding to one of the dimer configurations in the crystal structure of *Tm*TsaB alone (superposed in grey, PDB ID 2A6A), but was not observed in crystal structures of homologous TsaB structures. (**B**) Superimposition of *St*TobZ (PDB ID 3VEN; *St*TobZ-TsaD like in gray and *St*TobZ-YrdC like in black) and *Tm*TsaBDE (same color code as for Figure 2A).

uration' step during the reaction cycle. This kind of step could possibly be related to the release of reaction products or intermediates. However, affinities of TsaD for nucleotides and tRNA are moderate (22–24) and there is no evidence for the formation of stable intermediate/product complexes that would need assistance to release them from the enzyme. TsaE must therefore be involved in another step of the reaction cycle, for instance binding of the TC-AMP substrate. Inspection of *Tm*TsaBDE shows that TC-AMP has full access to the active site. Since the lability of the TC-AMP intermediate hampers its use in structural studies, we made a model of the *Ec*TsaBD -TC-AMP complex by superposing its AMP-moiety onto the *Ec*TsaBD-ADP complex (22) (Figure 4b). This model places the carbamoyl group of TC-AMP close to the Fe-ion. We then compared this model with substrate complexes of TobZ, which is a fusion protein of an TsaC- and a TsaD-like module (53). TobZ from *Streptoalloteichus tenebrarius* is responsible for the O-carbamoylation of tobramycin (an aminoglycoside related to kanamycin) to form nebramycin 5′. Its TsaC-module catalyses the formation of a carbamoyl-AMP intermediate, whose carbamoyl moiety is subsequently transferred to tobramycin by the TsaC-module. It was noticed that the active sites of TsaD and TobZ-TsaD are very similar (53). In TobZ complexes with carbamoyl-AMP and the acceptor tobramycin, the carbamoyl group is liganded to the Fe-ion and the tobramycin-OH group approached the Fe-bound phosphate (53). Superimposition of TobZ bound to carbamoyl-AMP and the acceptor tobramycin with our model of the TsaD/TC-AMP complex showed a perfect overlap between the carbamoyl-AMP moieties. The Fe-cluster can hence be proposed as a carbamoylation centre for all t^{6}A TC-transfer systems. Our HADDOCK model of the tRNA-TsaBD complex positions the N^6-amino group of the A37 anticodon base close to the carbamoyl group of TC-AMP and is well positioned for a nucleophilic attack of the TC-AMP carbonyl (Figure 4b). We hypothesize that the altered conformation of TsaD induced by TsaE could still allow binding of TC-AMP but not its chemical conversion. Superposition of TobZ onto TsaBDE, shows that the TsaC-like module of TobZ is bound to the TsaD-like module at the opposite side of TsaD compared with TsaE. TobZ contains a large central cavity that connects the active sites of the TsaC- and TsaD-like modules. This tunnel prevents diffusion of the unstable carbamoyl-phosphate intermediate into the bulk solution and channels it directly to the active site of the TsaD-like module (53). Similarly, binding of TsaC to TsaBDE in a manner that resembles the association of the TobZ TsaC and TsaD modules, would create a complex that could allow efficient transfer of TC-AMP from the active site of TsaC to that of TsaD. The role of TsaE might be to 'prepare' TsaD for interaction with TsaC. Complex formation between the four t^{6}A synthesis protein partners of *T. maritima* was observed by native gel shift experiments although a stable quaternary complex could not be isolated by gel filtration (23). For enzymatic purposes however, this complex would not need to be stable, but should only be sufficiently long-lived to permit TC-AMP transfer between TsaC and TsaD. Once the TC-AMP is bound, ATP could be hydrolysed by TsaE, promoting its dissociation from TsaBD, followed by binding of the tRNA substrate, renaturation of the TsaD metal binding sites and threonylcarbamoyl transfer to A37. The region around the active site that could be involved in TC-AMP channelling has conserved sequence patches (Supplementary Figure S7). The highly conserved SPT(F/Y)T loop of TsaE has its side chains in the coordination sphere of the γP of AMPCPP and is close to the threonylcarbamoyl moiety of TC-AMP in the TsaD active site. It is therefore well positioned to serve as a sensor to coordinate ATP hydrolysis and TC-AMP binding. A scheme representing the hypothetical role of TsaE during the t^{6}A reaction cycle is represented in Figure 6.

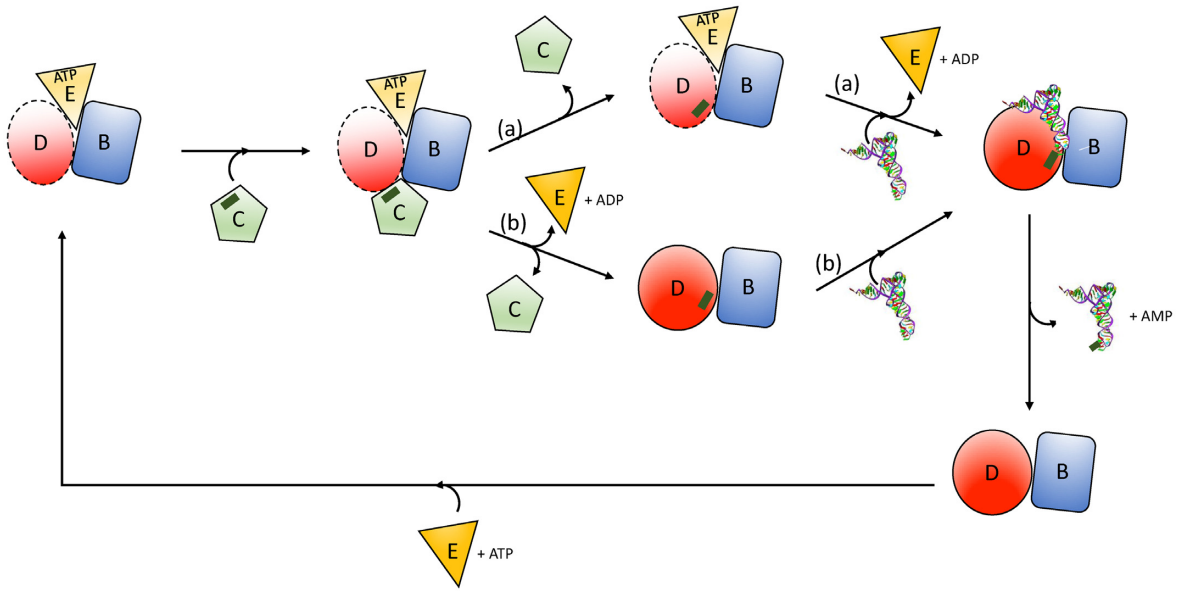

Figure 6. Hypothetic reaction scheme for TsaBDE. Binding of TsaE and ATP to TsaBD converts TsaD into an inactive conformation (symbolized by shady red colour). This conformation of TsaD then interacts with TsaC followed by transfer of TC-AMP (green stick) from TsaC to TsaD (pathways a or b). TsaE hydrolyses ATP and dissociates from TsaBD, liberating the binding site on TsaBD of the tRNA substrate. After transfer of the TC-moiety from TC-AMP to tRNA, the modified tRNA dissociates from TsaBD.

Comparison between bacterial TsaE and archaeal/eukaryotic Bud32

The threonyl-carbamoyl transferase multiprotein complexes in eukaryotes/archaea and bacteria have only the TC-transferring enzyme in common, Kae1 and TsaD respectively. Kae1 is flanked in the KEOPS complex by two subunits: Pcc1 binds to its N-terminal and Bud32 to its C-terminal domain (27,54). The helical bundle at the Pcc1-Kae1 interface mimics the TsaBD interface, despite the fact that Pcc1 and TsaB are unrelated. Pcc1 and TsaB likely play similar roles in the t^6A reaction pathway. Superposition of *Tm*TsaDE onto Kae1-Bud32 (Supplementary Figure S8) shows that TsaE and Bud32 both interact with the helical insertion of the C-terminal domain of TsaD and Kae1 respectively. TsaE however binds at the opposing end of TsaD compared to Bud32 and Kae1. Moreover, Bud32 does not block the access of tRNA to the active site of Kae1. The role of Bud32 in the t^6A reaction pathway has not been clarified so far. Bud32, resembles the small protein kinases of the Rio family, involved in the biogenesis of ribosomes (55). An ATPase-dependent role of the Rio proteins was suggested to regulate their dynamic association with pre ribosomal subunits (56). Inactivation of the active site of Bud32 is deleterious for yeast cells and also for t^6A activity of the KEOPS complex (14). It remains an open question whether TsaE and Bud32 are functional analogues or whether they play a different role in the t^6A reaction cycle.

CONCLUSION

Our data provide a structural rationale for the biochemical observations collected on *Ec*- and *Tm*TsaBDE, e.g. the competition between tRNA and TsaE for binding to TsaD. The structure of *Tm*TsaBDE confirms TsaE is not directly involved in the TC-transfer to tRNA, but suggests that it 'prepares' TsaD at the start of the reaction cycle. *Tm*TsaE converts *Tm*$TsaB_2D_2$ into an open form that could accept the TC-AMP intermediate from *Tm*TsaC2. After ATP hydrolysis, *Tm*TsaE dissociates from *Tm*TsaBD which switches to a closed active form, capable of binding metals and tRNA substrate. Then, modified tRNA leaves the active site and *Tm*TsaBD enters into a new reaction cycle. The open (inactive) and closed (active) form of *Tm*TsaBD might be in equilibrium in absence of *Tm*TsaE as suggested by SAXS data (23). It is tempting to correlate these two states with the observation that *Tm*TsaBD, in absence of *Tm*TsaE, catalyses a single turn-over tRNA modification. This equilibrium probably is species-dependent since it was not observed for *Ec*TsaBD (22).

It is of note that the TsaBDE complex offers an attractive target for antimicrobial drug development. Chemical compounds that either inhibit TsaE to bind to TsaBD or significantly stabilize the TsaBDE complex would have deleterious effects on t^6A activity and bacterial survival.

DATA AVAILABILITY

The coordinates of the *Tm*TsaBDE complex have been deposited at the PDB under the code 6FPE.

SUPPLEMENTARY DATA

Supplementary Data are available at NAR Online.

ACKNOWLEDGEMENTS

Sophia Missoury received a scholarship from the 'Fondation de la Recherche Médicale'. We thank the staff of the Proxima1 and 2 beamlines at the SOLEIL synchrotron for

assistance during the diffraction data collections. We are grateful to Marc Graille (Ecole Polytechnique, Palaiseau) and Tamara Basta (I2BC, Gif s/Yvette) for critical reading of the manuscript.

Authors Contributions: S.M., S.P., I.G., D.D., B.C., D.L., R.D. and W.Z. did the experimental work. S.M., B.C. and H.v.T. wrote the paper.

FUNDING

This work received support from the French Infrastructure for Structural Biology [FRISBI ANR-10-INSB-0501]. Funding for open access charge: lab budget.
Conflict of interest statement. None declared.

REFERENCES

1. Grosjean,H. (2009) *DNA and RNA Modification Enzymes: Structure, Mechanism, Function and Evolution*.Landes Bioscience, Austin, pp. 1–18.
2. Machnicka,M.A., Milanowska,K., Oglou,O.O., Purta,E., Kurkowska,M., Olchowik,A., Januszewski,W., Kalinowski,S., Dunin-Horkawicz,S., Rother,K.M. *et al.* (2013) MODOMICS: a database of RNA modification pathways - 2013 update. *Nucleic Acids Res.*, **41**, D262–D267.
3. Thiaville,P.C., El Yacoubi,B., Köhrer,C., Thiaville,J.J., Deutsch,C., Iwata-Reuyl,D., Bacusmo,J.M., Armengaud,J., Bessho,Y., Wetzel,C. *et al.* (2015) Essentiality of threonylcarbamoyladenosine (t6A), a universal tRNA modification, in bacteria. *Mol. Microbiol.*, **98**, 1199–1221.
4. El Yacoubi,B., Bailly,M. and de Crécy-Lagard,V. (2012) Biosynthesis and function of posttranscriptional modifications of transfer RNAs. *Annu. Rev. Genet.*, **46**, 69–95.
5. Grosjean,H., de Crécy-Lagard,V. and Marck,C. (2010) Deciphering synonymous codons in the three domains of life: co-evolution with specific tRNA modification enzymes. *FEBS Lett.*, **584**, 252–264.
6. Morin,A., Auxilien,S., Senger,B., Tewari,R. and Grosjean,H. (1998) Structural requirements for enzymatic formation of threonylcarbamoyladenosine (t6A) in tRNA: an in vivo study with Xenopus laevis oocytes. *RNA*, **4**, 24–37.
7. Murphy,F.V., Ramakrishnan,V., Malkiewicz,A. and Agris,P.F. (2004) The role of modifications in codon discrimination by tRNALysUUU. *Nat. Struct. Mol. Biol.*, **11**, 1186–1191.
8. Braun,D.A., Rao,J., Mollet,G., Schapiro,D., Daugeron,M.C., Tan,W., Gribouval,O., Boyer,O., Revy,P., Jobst-Schwan,T. *et al.* (2017) Mutations in KEOPS-complex genes cause nephritic syndrome with primary microcephaly. *Nat. Genet.*, **49**, 1529–1538.
9. Edvardson,S., Prunetti,L., Arraf,A., Haas,D., Bacusmo,J.M., Hu,J.F., Ta-Shma,A., Dedon,P.C., De Crécy-Lagard,V. and Elpeleg,O. (2017) TRNA N6-adenosine threonylcarbamoyltransferase defect due to KAE1/TCS3 (OSGEP) mutation manifest by neurodegeneration and renal tubulopathy. *Eur. J. Hum. Genet.*, **25**, 545–551.
10. Deutsch,C., El Yacoubi,B., De Crécy-Lagard,V. and Iwata-Reuyl,D. (2012) Biosynthesis of threonylcarbamoyl adenosine (t6A), a universal tRNA nucleoside. *J. Biol. Chem.*, **287**, 13666–13673.
11. El Yacoubi,B., Lyons,B., Cruz,Y., Reddy,R., Nordin,B., Agnelli,F., Williamson,J.R., Schimmel,P., Swairjo,M.A. and De Crécy-Lagard,V. (2009) The universal YrdC/Sua5 family is required for the formation of threonylcarbamoyladenosine in tRNA. *Nucleic Acids Res.*, **37**, 2894–2909.
12. Wan,L.C.K., Mao,D.Y.L., Neculai,D., Strecker,J., Chiovitti,D., Kurinov,I., Poda,G., Thevakumaran,N., Yuan,F., Szilard,R.K. *et al.* (2013) Reconstitution and characterization of eukaryotic N6-threonylcarbamoylation of tRNA using a minimal enzyme system. *Nucleic Acids Res.*, **41**, 6332–6346.
13. Lauhon,C.T. (2012) Mechanism of N6-threonylcarbamoyladenonsine (t6A) biosynthesis: isolation and characterization of the intermediate threonylcarbamoyl-AMP. *Biochemistry*, **51**, 8950–8963.
14. Srinivasan,M., Mehta,P., Yu,Y., Prugar,E., Koonin,E.V., Karzai,A.W. and Sternglanz,R. (2011) The highly conserved KEOPS/EKC complex is essential for a universal tRNA modification, t6A. *EMBO J.*, **30**, 873–881.
15. El Yacoubi,B., Hatin,I., Deutsch,C., Kahveci,T., Rousset,J.P., Iwata-Reuyl,D., G Murzin,A. and De Crécy-Lagard,V. (2011) A role for the universal Kae1/Qri7/YgjD (COG0533) family in tRNA modification. *EMBO J.*, **30**, 882–893.
16. Downey,M., Houlsworth,R., Maringele,L., Rollie,A., Brehme,M., Galicia,S., Guillard,S., Partington,M., Zubko,M.K., Krogan,N.J. *et al.* (2006) A Genome-Wide screen identifies the evolutionarily conserved KEOPS complex as a telomere regulator. *Cell*, **124**, 1155–1168.
17. Kisseleva-Romanova,E., Lopreiato,R., Baudin-Baillieu,A., Rousselle,J.C., Ilan,L., Hofmann,K., Namane,A., Mann,C. and Libri,D. (2006) Yeast homolog of a cancer-testis antigen defines a new transcription complex. *EMBO J.*, **25**, 3576–3585.
18. Perrochia,L., Crozat,E., Hecker,A., Zhang,W., Bareille,J., Collinet,B., Van Tilbeurgh,H., Forterre,P. and Basta,T. (2013) In vitro biosynthesis of a universal t6A tRNA modification in Archaea and Eukarya. *Nucleic Acids Res.*, **41**, 1953–1964.
19. Wan,L.C.K., Maisonneuve,P., Szilard,R.K., Lambert,J.P., Ng,T.F., Manczyk,N., Huang,H., Laister,R., Caudy,A.A., Gingras,A.C. *et al.* (2017) Proteomic analysis of the human KEOPS complex identifies C14ORF142 as a core subunit homologous to yeast Gon7. *Nucleic Acids Res.*, **45**, 805–817.
20. Zhang,W., Collinet,B., Graille,M., Daugeron,M.C., Lazar,N., Libri,D., Durand,D. and Van Tilbeurgh,H. (2015) Crystal structures of the Gon7/Pcc1 and Bud32/Cgi121 complexes provide a model for the complete yeast KEOPS complex. *Nucleic Acids Res.*, **43**, 3358–3372.
21. Handford,J.I., Ize,B., Buchanan,G., Butland,G.P., Greenblatt,J., Emili,A. and Palmer,T. (2009) Conserved network of proteins essential for bacterial viability. *J. Bacteriol.*, **191**, 4732–4749.
22. Zhang,W., Collinet,B., Perrochia,L., Durand,D. and Van Tilbeurgh,H. (2015) The ATP-mediated formation of the YgjD-YeaZ-YjeE complex is required for the biosynthesis of tRNA t6A in Escherichia coli. *Nucleic Acids Res.*, **43**, 1804–1817.
23. Luthra,A., Swinehart,W., Bayooz,S., Phan,P., Stec,B., Iwata-Reuyl,D. and Swairjo,M.A. (2018) Structure and mechanism of a bacterial t6A biosynthesis system. *Nucleic Acids Res.*, **46**, 1395–1411.
24. Nichols,C.E., Lamb,H.K., Thompson,P., El Omari,K., Lockyer,M., Charles,I., Hawkins,A.R. and Stammers,D.K. (2013) Crystal structure of the dimer of two essential Salmonella typhimurium proteins, YgjD & YeaZ and calorimetric evidence for the formation of a ternary YgjD-YeaZ-YjeE complex. *Protein Sci.*, **22**, 628–640.
25. Xu,Q., McMullan,D., Jaroszewski,L., Krishna,S.S., Elsliger,M.A., Yeh,A.P., Abdubek,P., Astakhova,T., Axelrod,H.L., Carlton,D. *et al.* (2010) Structure of an essential bacterial protein YeaZ (TM0874) from Thermotoga maritima at 2.5 Å resolution. *Acta Crystallogr. Sect. F Struct. Biol. Cryst. Commun.*, **66**, 1230–1236.
26. Vecchietti,D., Ferrara,S., Rusmini,R., Macchi,R., Milani,M. and Bertoni,G. (2016) Crystal structure of YeaZ from Pseudomonas aeruginosa. *Biochem. Biophys. Res. Commun.*, **470**, 460–465.
27. Mao,D.Y.L., Neculai,D., Downey,M., Orlicky,S., Haffani,Y.Z., Ceccarelli,D.F., Ho,J.S.L., Szilard,R.K., Zhang,W., Ho,C.S. *et al.* (2008) Atomic structure of the KEOPS Complex: An ancient protein Kinase-Containing molecular machine. *Mol. Cell*, **32**, 259–275.
28. Teplyakov,A., Obmolova,G., Tordova,M., Thanki,N., Bonander,N., Eisenstein,E., Howard,A.J. and Gilliland,G.L. (2002) Crystal structure of the YjeE protein from Haemophilus influenzae: a putative ATpase involved in cell wall synthesis. *Proteins Struct. Funct. Genet.*, **48**, 220–226.
29. Nguyen,H.A., El Khoury,T., Guiral,S., Laaberki,M.H., Candusso,M.P., Galisson,F., Foucher,A.E., Kesraoui,S., Ballut,L., Vallet,S. *et al.* (2017) Expanding the kinome World: a new protein kinase family widely conserved in bacteria. *J. Mol. Biol.*, **429**, 3056–3074.
30. Wan,L.C.K., Pillon,M.C., Thevakumaran,N., Sun,Y., Chakrabartty,A., Guarné,A., Kurinov,I., Durocher,D. and Sicheri,F. (2016) Structural and functional characterization of KEOPS dimerization by Pcc1 and its role in t6A biosynthesis. *Nucleic Acids Res.*, **44**, 6971–6980.
31. Perrochia,L., Guetta,D., Hecker,A., Forterre,P. and Basta,T. (2013) Functional assignment of KEOPS/EKC complex subunits in the

biosynthesis of the universal t6A tRNA modification. *Nucleic Acids Res.*, **41**, 9484–9499.
32. Lerner,C.G., Hajduk,P.J., Wagner,R., Wagenaar,F.L., Woodall,C., Gu,Y.-G., Searle,X.B., Florjancic,A.S., Zhang,T., Clark,R.F. *et al.* (2007) From bacterial genomes to novel antibacterial agents: discovery, characterization, and antibacterial activity of compounds that bind to HI0065 (YjeE) from Haemophilus influenzae. *Chem. Biol. Drug Des.*, **69**, 395–404.
33. Collinet,B., Friberg,A., Brooks,M.A., van den Elzen,T., Henriot,V., Dziembowski,A., Graille,M., Durand,D., Leulliot,N., Saint André,C. *et al.* (2011) Strategies for the structural analysis of multi-protein complexes: lessons from the 3D-Repertoire project. *J. Struct. Biol.*, **175**, 147–158.
34. Gaspar,P., Oliveira,J.L., Frommlet,J., Santos,M.A.S. and Moura,G. (2012) EuGene: Maximizing synthetic gene design for heterologous expression. *Bioinformatics*, **28**, 2683–2684.
35. Kabsch,W. (2010) XDS. *Acta Crystallogr. Sect. D*, **66**, 125–132.
36. McCoy,A.J., Grosse-Kunstleve,R.W., Adams,P.D., Winn,M.D., Storoni,L.C. and Read,R.J. (2007) Phaser crystallographic software. *J. Appl. Crystallogr.*, **40**, 658–674.
37. Winn,M.D., Ballard,C.C., Cowtan,K.D., Dodson,E.J., Emsley,P., Evans,P.R., Keegan,R.M., Krissinel,E.B., Leslie,A.G.W., McCoy,A. *et al.* (2011) Overview of the CCP4 suite and current developments. *Acta Crystallogr. Sect. D Biol. Crystallogr.*, **67**, 235–242.
38. Webb,B. and Sali,A. (2014) Comparative protein structure modeling using MODELLER. *Curr. Protoc. Bioinforma.*, **2014**, 5.6.1–5.6.32.
39. Adams,P.D., Afonine,P.V., Bunkóczi,G., Chen,V.B., Echols,N., Headd,J.J., Hung,L.W., Jain,S., Kapral,G.J., Grosse Kunstleve,R.W. *et al.* (2011) The Phenix software for automated determination of macromolecular structures. *Methods*, **55**, 94–106.
40. Emsley,P., Lohkamp,B., Scott,W.G. and Cowtan,K. (2010) Features and development of Coot. *Acta Crystallogr. Sect. D Biol. Crystallogr.*, **66**, 486–501.
41. Van Zundert,G.C.P., Rodrigues,J.P.G.L.M., Trellet,M., Schmitz,C., Kastritis,P.L., Karaca,E., Melquiond,A.S.J., Van Dijk,M., De Vries,S.J. and Bonvin,A.M.J.J. (2016) The HADDOCK2.2 Web Server: User-Friendly integrative modeling of biomolecular complexes. *J. Mol. Biol.*, **428**, 720–725.
42. Sankaranarayanan,R., Dock-Bregeon,A.C., Romby,P., Caillet,J., Springer,M., Rees,B., Ehresmann,C., Ehresmann,B. and Moras,D. (1999) The structure of threonyl-tRNA synthetase-tRNAThrcomplex enlightens its repressor activity and reveals an essential zinc ion in the active site. *Cell*, **97**, 371–381.
43. Ashkenazy,H., Erez,E., Martz,E., Pupko,T. and Ben-Tal,N. (2010) ConSurf 2010: calculating evolutionary conservation in sequence and structure of proteins and nucleic acids. *Nucleic Acids Res.*, **38**, W529–W533.
44. Crooks,G.E., Hon,G., Chandonia,J.M. and Brenner,S.E. (2004) WebLogo: a sequence logo generator. *Genome Res.*, **14**, 1188–1190.
45. Krissinel,E. and Henrick,K. (2004) Secondary-structure matching (PDBeFold), a new tool for fast protein structure alignment in three dimensions. *Acta Cryst.*, **D60**, 2256–2268.
46. DeLano,W.L. (2014) The PyMOL molecular graphics system, version 1.8. *Schrödinger LLC*, doi:10.1038/hr.2014.17.
47. Dolinsky,T.J., Nielsen,J.E., McCammon,J.A. and Baker,N.A. (2004) PDB2PQR: an automated pipeline for the setup of Poisson-Boltzmann electrostatics calculations. *Nucleic Acids Res.*, **32**, W665–W667.
48. Pettersen,E.F., Goddard,T.D., Huang,C.C., Couch,G.S., Greenblatt,D.M., Meng,E.C. and Ferrin,T.E. (2004) UCSF Chimera—a visualization system for exploratory research and analysis. *J. Comput. Chem*, **25**, 1605–1612.
49. Hecker,A., Leulliot,N., Gadelle,D., Graille,M., Justome,A., Dorlet,P., Brochier,C., Quevillon-Cheruel,S., Le Cam,E., van Tilbeurgh,H. *et al.* (2007) An archaeal orthologue of the universal protein Kae1 is an iron metalloprotein which exhibits atypical DNA-binding properties and apurinic-endonuclease activity in vitro. *Nucleic Acids Res.*, **35**, 6042–6051.
50. Cherfils,J. and Zeghouf,M. (2013) Regulation of small GTPases by GEFs, GAPs, and GDIs. *Physiol. Rev.*, **93**, 269–309.
51. Hanks,S., Quinn,A. and Hunter,T. (1988) The protein kinase family: conserved features and deduced phylogeny of the catalytic domains. *Science*, **241**, 42–52.
52. Aydin,I., Saijo-Hamano,Y., Namba,K., Thomas,C. and Roujeinikova,A. (2011) Structural analysis of the essential resuscitation promoting factor yeaz suggests a mechanism of nucleotide regulation through dimer reorganization. *PLoS One*, **6**, e23245.
53. Parthier,C., Görlich,S., Jaenecke,F., Breithaupt,C., Bräuer,U., Fandrich,U., Clausnitzer,D., Wehmeier,U.F., Böttcher,C., Scheel,D. *et al.* (2012) The O-carbamoyltransferase TobZ catalyzes an ancient enzymatic reaction. *Angew. Chem. Int. Ed.*, **51**, 4046–4052.
54. Hecker,A., Lopreiato,R., Graille,M., Collinet,B., Forterre,P., Libri,D. and van Tilbeurgh,H. (2008) Structure of the archaeal Kae1/Bud32 fusion protein MJ1130: a model for the eukaryotic EKC/KEOPS subcomplex. *EMBO J.*, **27**, 2340–2351.
55. LaRonde-LeBlanc,N. and Wlodawer,A. (2005) A family portrait of the RIO kinases. *J. Biol. Chem.*, **280**, 37297–37300.
56. Knüppel,R., Christensen,R.H., Gray,F.C., Esser,D., Strauß,D., Medenbach,J., Siebers,B., MacNeill,S.A., LaRonde,N. and Ferreira-Cerca,S. (2018) Insights into the evolutionary conserved regulation of Rio ATPase activity. *Nucleic Acids Res.*, **46**, 1441–1456.